Publ. Astron. Obs. Belgrade No. 91 (2012), 21 - 34 *Invited review*

SPECTRO-INTERFEROMETRY AND DIFFERENTIAL INTERFEROMETRY WITH AMBER AND THE VLTI

R. G. PETROV

Laboratoire Lagrange, UMR 7293, University of Nice Sophia-Antipolis, CNRS, Observatoire de la Côte d'Azur, BP 4229, 06304 Nice Cedex 4, France
E–mail: romain.petrov@unice.fr

1. INTRODUCTION

In the last 10 years, Optical Long Baseline Interferometry (OLBI) has entered a phase of sustained scientific production, with more than 450 refereed science papers, which represents more than 75% of the science production of optical interferometry since the first observations (Michelson & Pease 1921). One of the reasons of this success is that major interferometers, such as the Keck Interferometer (http://www.keckobservatory.org, Colavita et al. 2003, Colavita et al. 2004), CHARA and the VLTI have "general user oriented" instruments ". Strictly speaking, only the VLTI instruments are truly "general user" with calls for proposals to all the astronomic community (with a priority but not an exclusivity to ESO member states). This contributes to the fact that the VLTI has produced more than 60% of the interferometric science results since the beginning of optical interferometry (http://olbin.jpl.nasa.gov/). However, the KI and CHARA are also open to a broad community of scientists. This strong scientific output is being obtained in spite of the fact that optical interferometers produce regularly images only since 2008, and so far less than 15% of the science papers have been based on interferometric imaging.

However, the community of science users of OLBI is growing slowly, and the technique is not yet considered as just "one of the observing tools" available for the astrophysicist, even when it is applicable to his targets of interests. One of the goals of this paper is to insist on the proximity between optical interferometry and other observing techniques such as spectroscopy.

Almost all current OLBI focal instruments are equipped with more or less ambitious spectrographs and are actually spectro-interferometers. We want to illustrate the fact that spectro interferometry is much more than interferometry providing spatial information in different spectral channels. In fact, the cross analysis of the interferometric information obtained simultaneously in different spectral channels, sometimes called Differential Interferometry (DI) (Petrov 1989) or, more recently, Self Phase Referencing Interferometry (Woillez et al. 2012), yields much more information than the sequential analysis in different spectral channels.

A spectro-interferometric focal instrument gives access to several wavelength dependent interferometric observables:

– The absolute visibility as a function of λ: $V(\lambda)$.
– The closure phase $\Psi(\lambda)$ if we have at least three telescopes.
– The differential visibility $V(\lambda)/ < V(\lambda) >$
– The differential phase $\phi(\lambda) - < \phi(\lambda) >$
– The spectrum $s(\lambda)$

The first two measurables are the "standard" optical interferometry measures. The last three are specific to spectro-interferometry and include the spectrum that is a key calibration when it is obtained from the interferometric instrument itself.

In this paper we will briefly define these measures and illustrate their use and potential in the case of the VLTI focal instrument AMBER, whose main characteristics are very briefly recorded in the annex, and emphasize the specific potential of differential interferometry.

2. OPTICAL INTERFEROMETRY AND ITS OBSERVABLES

A multiple aperture interferometer consists of several telescopes separated by baseline B_{ij}, combined for the light coming through each telescopes to arrive at the combined focal plane after traveling an equal optical path. When the optical path difference (OPD) is made shorter than the coherence length $C=R\lambda$ (where R is the spectral resolution) the interferometer is said to be "coherenced". When the OPDs are equalized to a small fraction of λ, the interferometer is cophased. In both cases, the focal instrument observes one system of fringes for each baseline, physically identical to the Young fringes of our high school classes in optics. An interferometric measurement at wavelength λ yields the complex visibility of the source brightness distribution $o(\underline{r},\lambda)$ which is the Fourier transform $O(\underline{u},\lambda)$ of $o(\underline{r},\lambda)$, at the spatial frequency $\underline{B}_{ij}/\lambda$. The variable $\underline{r}$ is an angular vector, $\underline{u}$ is its Fourier transform conjugate, called the spatial frequency and $\underline{B}_{ij}$ is the baseline projected on the sky. The modulus $V(\lambda)$ of $O(\underline{u},\lambda)$, called source visibility, is given by the contrast of the fringes and its phase $\phi(\lambda)$ should be given by the position of the fringes. If we have enough baselines to pave the frequency plane (often called the u-v plane) with a step f within a diameter B_{max}, the Fourier inversion of $O(\underline{u},\lambda)$ yields the brightness distribution $o(\underline{r},\lambda)$ with an angular resolution λ/B_{max} within a field $F=\lambda/f$. Obtaining all these measurements is called synthetizing the aperture of diameter B_{max}. Beyond the technical difficulty in combining all these beams with a zero OPD difference, in spite of the variable atmospheric OPD and instrument vibrations, aperture synthesis faces two severe difficulties.

– Synthesizing an aperture much larger than the individual telescopes requires a very large number of baselines and if the interferometer has only a small number of telescopes, this is a very long process based on telescope relocations, helped by projected baseline rotation with the hour angle (the super synthesis). In practice we have to reconstruct images with a very poorly covered u-v plane and we face a difficult "underdetermined" inverse problem.

– Knowing the absolute phase of the fringes would require an absolute measure of the optical paths of all beams through the atmosphere and then the interferometer. This is impossible in practice, except when a reference source is available within a very small field and the relative metrology between the science and the reference source is perfectly measured. This technique, called "phase referencing" is very difficult to

implement and has given only very limited results so far. The second-generation VLTI instrument GRAVITY is dedicated to this approach, in the very special conditions of the Galactic center, where a bright enough reference source exists close enough to many of the targets of interest. So far we have access only to:

◦ The closure phases $\Psi_{ijk}(\lambda) = \phi_{ij}(\lambda)+\phi_{jk}(\lambda)+\phi_{ik}(\lambda)$ that combines three baselines in a way that eliminates the optical paths introduced in each beam. The closure phase is partial phase information. If the u-v coverage is very dense, the closure phases can be combined to retrieve the phases and hence the object image, but this makes the "inverse problem" even more "underdetermined", particularly when we have a small number of telescopes. It is also obvious that the technique can be applied only when the interferometer has at least three telescopes.

◦ The differential phase, specific to differential interferometry, which measures all the phases relatively to the phase of a reference channel (usually the average over all available channels): $\phi_d(\lambda) = \phi(\lambda) - \phi_{ref}$. If the phase in the reference channel is known, for example because we know that the source can be considered as a point source in a given spectral channel, or group of spectral channels, the differential phase yields the actual phase, and the object is its own "phase reference", which explains the term "self phase referencing". When the reference phase is unknown, the use of differential phases reduces dramatically the number of unknowns in the "inverse problem". For many classes of objects, we will show that the differential phase yields specific information even without absolute visibility and phase measurements.

3. ABSOLUTE VISIBILITY

The absolute visibility $V_{ij}(\lambda)$ is the modulus of the source complex visibility $O(\underline{u},\lambda)$, which is the Fourier transform of its brightness distribution $o(\underline{r},\lambda)$. For simple objects, the absolute visibility constrains the equivalent size of the source in the direction of the baseline B_{ij}. $V(\lambda)$ is deduced from the contrast of the interferometric fringes, which depends also from instrument and atmospheric parameters. The "instrumental contrast" is eliminated by the use of a "calibrator", i.e. a source of known visibility such as a point source or a disk with known diameter. This calibration assumes that the conditions are exactly the same during the observation of the calibration and science sources, which is very seldom the case. As a consequence $V(\lambda)$ is usually difficult to calibrate and the accuracy limit is of the order of 3% with AMBER, mainly because the large dispersed interferograms of AMBER need relatively long frame times, which makes the experiment sensitive to changes in the fast OPD variations enhanced by the UT variable vibrations. Some instruments, such as VINCI and maybe PIONEER (see annex 1), which have much shorter frame times, yield more accurate absolute visibilities, of the order of 1%. Figure 1a illustrates an important result of the VLTI using broadband absolute visibilities only. From visibility measurements in a large number of directions, obtained using two AT locations (E0-G1=66m NNW and B3-M0=140m ENE), it has been possible to estimate the equivalent angular size of the rapidly rotating star Altair in many directions. The resulting ratio between polar and equatorial directions has been found to 1.56, which could not be explained by any rotational flattening and was hence considered as the first direct measurement of the Von Zeipel effect, which links brightness and local gravitation and hence predicts that the pole of a rapid rotator is brighter than the equator (Domiciano de Souza et al. 2005).

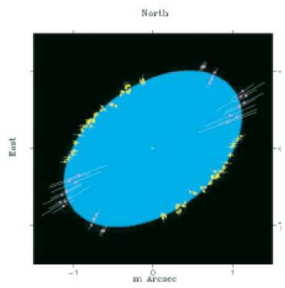

Figure 1a: equivalent diameter of Altair as a function of the position angle, measured by the VLTI/VINCI. The diameter ratio of 1.56 could be explained only by Von Zeipel gravitational darkening

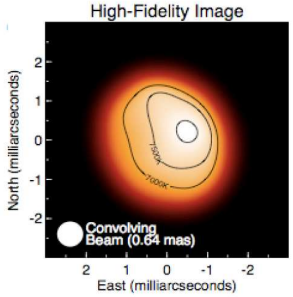

Figure 1b: CHARA "temperature" image reconstruction of Altair, using many absolute visibilities and closure phases. The pole appears clearly brighter, as an "objective image" confirmation of the Von Zeipel effect

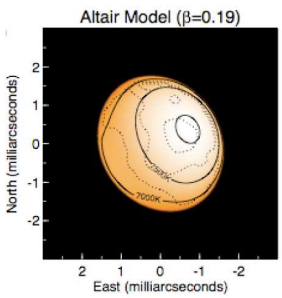

Figure 1c: Model of the Von Zeipel effect on Altair

From Domiciano de Souza et al, 2005

From Monnier et al, 2008

Figure 1: A major success of broad band interferometry: the Von Zeipel gravitational darkening on the rapid rotator Altair.

4. CLOSURE PHASE

The closure phase $\Psi_{\rm ijk}(\lambda)$ is the combination of the phase measured on three baselines: $\Psi_{\rm ijk}(\lambda) = \phi_{\rm ij}(\lambda) + \phi_{\rm jk}(\lambda) + \phi_{\rm ki}(\lambda)$. Radio interferometry has shown that this quantity is independent from the optical path in each one of the beams. Combining many closure phases allows to rebuilt phase information and hence images as illustrated in figure 1b and 1c, showing the reconstruction of the image of Altair from many 4 telescopes CHARA/MIRC observations (Monnier et al. 2007). The hotter and hence brighter pole appears in this "objective image" and allows to confirm and to quantify the Von Zeipel interpretation.

In single band interferometry, visibilities and closure phases on as many baseline triplets as possible are combined to allow an image reconstruction. A standard claim is that the u-v coverage filling is by far the most important factor for the quality of the image, well before visibility and closure phase accuracies. This is illustrated, for example, by Benisty et al, (2011) where more than 30 poor accuracy (5° to 15° errors) closure phases have been used to obtain with AMBER one of the best skewed disk images of the inner rim of a dust accretion disk.

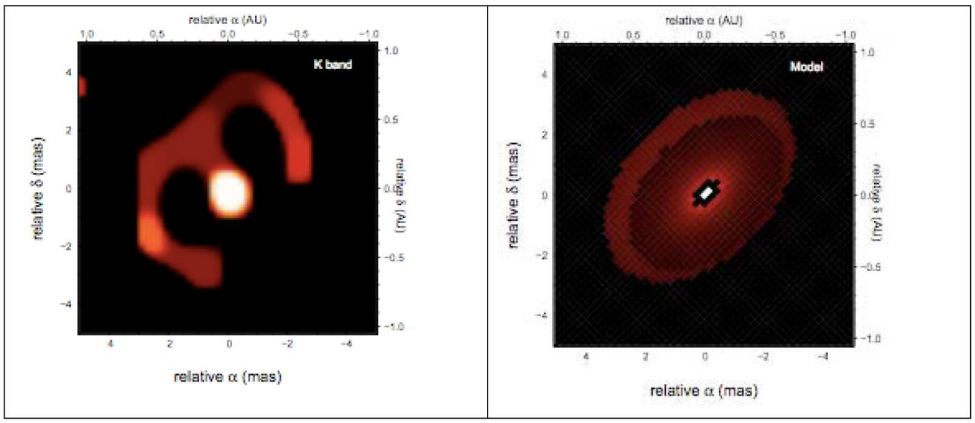

Figure 2: AMBER image (left) and model (right) of HR 5999 in the K band, showing the inner rim of the accretion disk, with a face on rim much brighter. This image has been obtained by combining more than 30 relatively mediocre quality measurements on visibilities and closure phase with VLTI -AT triplets with AMBER (from Benisty, M, et al., A&A, 2011).

The same processing can be repeated in many narrower spectral channels as illustrated by Chiavassa et al (2010), which displays AMBER images of the cool late type star VX Sgr, in 5 spectral bands in H and K and reveals extended molecular layer dominated by water vapor at 2 μm and 2.35-2.5 μm together with two hot spots with a maximum contrast in the H band. It is worth noting, that in this case, the major and more reliable information is the variation of diameter and spot contrast as a function of the wavelength, which would have been much better constrained by differential measures, as illustrated in the next sections.

5. DIFFERENTIAL VISIBILITY

To compensate the large errors on the absolute visibility, one can self calibrate the visibility with regard to the visibility in a particular channel or, more often, with regard to the broadband visibility. The key advantage is that the differential visibility $V(\lambda)/ <V(\lambda) >$ is much more accurate (assuming that some specific artifacts are corrected: Petrov et al. 2012). Typically, AMBER differential visibilities can be measured with accuracy better than 1%, even on very faint sources like the quasar 3C273, where absolute visibilities have uncertainties much higher than 5%. On simple objects, the differential visibility indicates the relative size variations between several spectral channels. Malbet et al. (2007) illustrated this on the Herbig star MWC 297. During the first commissioning of AMBER we observed this target with a strong Brγ emission line to check our medium resolution spectral calibration. The data processing, revealed a drop in visibility (figure 3a) in the spectral line, which was found to be very significant scientifically and yield the first AMBER science result. From the Spectral Energy Distribution (SED) we knew that this star has a dust accretion disk. The emission line reveals the presence of a gas wind, with some constraints on its overall velocity field, but we had no constraints on its size, and it was therefore

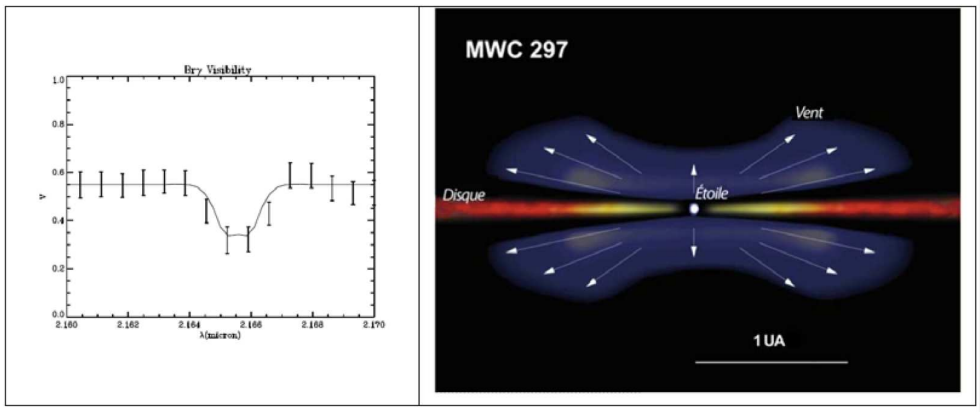

Figure 3: First AMBER observation of the Herbig star MWC 297, from Malbet at al., A&A 2007. Left: visibility as a function of λ, with a drop of visibility in the Brγ line showing that the wind is produced above the inner part of a geometrically thin but optically thick dust disk. The model used all information from other observation techniques and in particular the spectral line profile and the SED.

impossible to understand where the wind was produced. The drop in visibility in the line shows that the gas wind is produced in a region more extended than the inner rim of the dust disc. To explain the visibility drop, the SED and the line profile, we had to conclude that this star has a wind with a wide opening angle produced above the inner part of the dust disk, which had to be geometrically thin and optically thick as shown by the model in figure 3b. The model was later confirmed and of course very substantially refined by much more detailed observations, including many differential and closure phases by Weigelt et al., (2011).

This result illustrates the power of a single interferometric measure, which removes the degeneracy of many parameters of the model of an object already investigated by other observation techniques. It also shows that interferometric quantities can be fairly easy to use conceptually: a simple constraint of the FWHM of the wind constrains strongly its relationship with the dust, which was a topic strongly debated before. There are many other examples of similar results. The most recent one is our measurement of the differential visibility in the Paα broad emission line on the 3C273 quasar (Petrov et al. 2012), which reveals a visibility drop in the line, which increases with the baseline. The BLR seen by interferometry is therefore larger than 0.4 mas, i.e. 1200 ld, in radius, than the inner rim of the dust torus (0.3 mas) and much larger than the 300 ld (0.1 mas) radius measured from standard Reverberation Mapping (RM). A BLR with reverberation mapping radius would have produced an increase of the visibility in the line, of about 3% while our accuracy is of the order of 1% and we see a visibility drop of about 8%. This also illustrate the power of super resolution of accurate (differential) visibility measurements, since we put strong constraints on the sizes of structures ranging from 0.1 to 0.4 mas with an interferometer with resolution λ/B>3.5 mas.

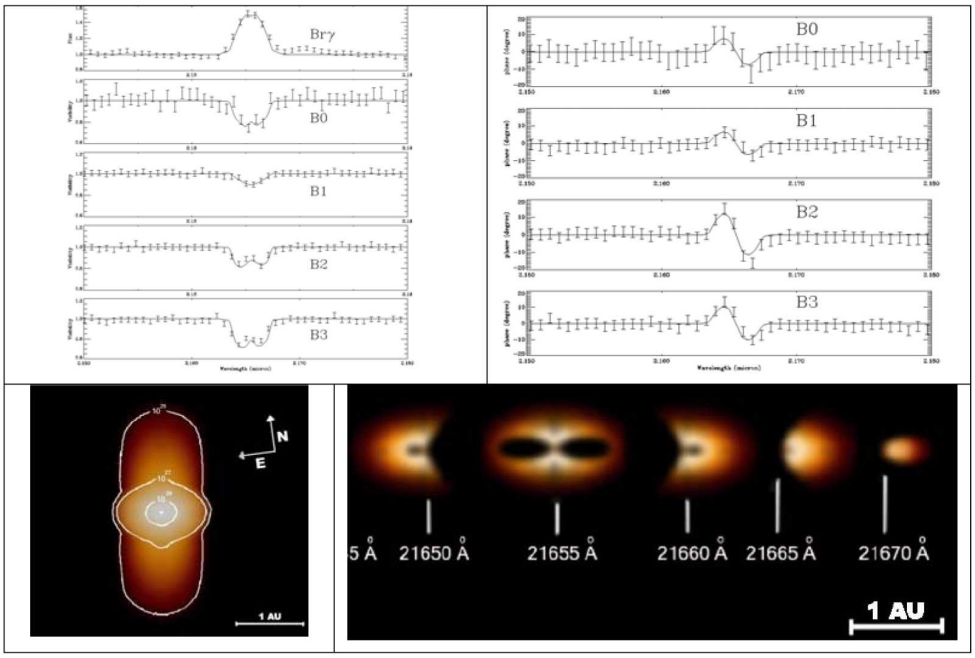

Figure 4: AMBER/VLTI observations of the classical Be star αArae, from Meilland et al., A&A2007. Top, spectrum and differential visibility (left) and differential phases (right) observed through the Brγ emission line. Both differential visibility and phase have the shape predicted for a rotating disk. Bottom left: the global brightness map, from a model fitting of all measures with the SIMECA code. Bottom right, narrow band images, in the wing of the emission line. The differential visibility yields the relative size of each "equal velocity" bin, and the differential phase yields its position. This position showed that the velocity field is Keplerian.

6. DIFFERENTIAL PHASE

The absolute phase is usually not accessible in optical interferometry since it needs an off axis reference source, which is seldom available, and additional complex hardware to measure accurately the differential OPD between the two sources. In spectro-interferometry and differential interferometry we can use the differential phase $\phi(\lambda) - < \phi(\lambda) >$. In practice we do not only subtract the average phase, but also the average slope of the phase, as explained for example in Petrov (2007) and Petrov (2012). For simple objects (and it is often possible to select reference spectral bins where the object is quite simple), the differential phase indicates the relative position of the object in the two spectral channels, as well as their relative intensity . The amplitude of the differential phase alone cannot separate these two effects, but if the object is even only marginally resolved, the combination of differential visibility and phase constraints both values. The first and very emblematic result of differential phase was the analysis of the geometry and the kinematics of the wind around the classical Be star α Arae, by Meilland et al. (2007), as illustrated by figure 4, which displays the

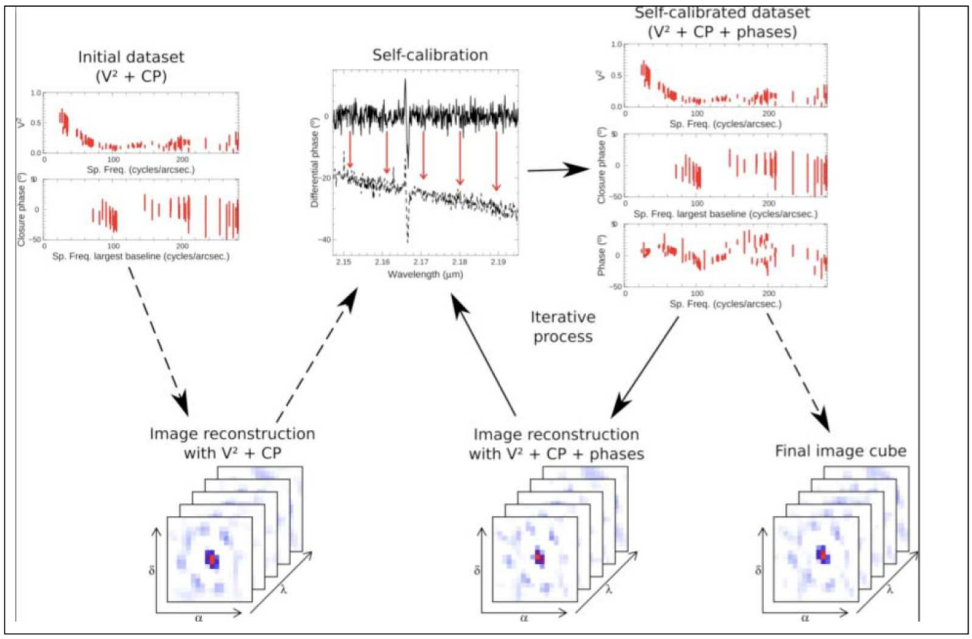

Figure 5: From Millour et al, A&A 2011: Principle of the polychromatic image reconstruction.

spectrum, the differential visibility and the differential phase observed through the Brγ emission line. Both differential visibility and phase have the shape predicted for a rotating Keplerian disk (Stee 1966).

7. DIFFERENTIAL PHASE AND POLYCHROMATIC IMAGING.

As we have discussed in the introduction, one of the main difficulties in interferometric imaging is to reconstruct the phase of the object. As early as 2004, we proposed a self-calibration scheme which has been developed by Millour et al., (2011) as it illustrated in figures 5 and 6. The figure 5 illustrates the principle of this self calibration of phases. Since we have the differential phases, the phase unknowns are reduced to the phases of the reference channels, which are constrained only by closure phase measures. The first step is to perform a standard (or "classical") image reconstruction using the visibility and closure phase. This gives an estimate of the object in the continuum, which is the reference channel, and hence of its phase. From this phase in the reference channel and the differential phase, we compute the absolute phase, and we proceed in a similar way with the visibility, combining the differential visibility and the visibility in the reference channel from the first image. Then, we perform an image reconstruction with full phases and improved visibilities. This gives a new image of the source in the reference channel, and a new iteration can be started, until the phase stops to evolve and we obtain the final image data cube. We believe that this approach is fairly general and can be used for any type of objects, including with strong differences between all individual channels.

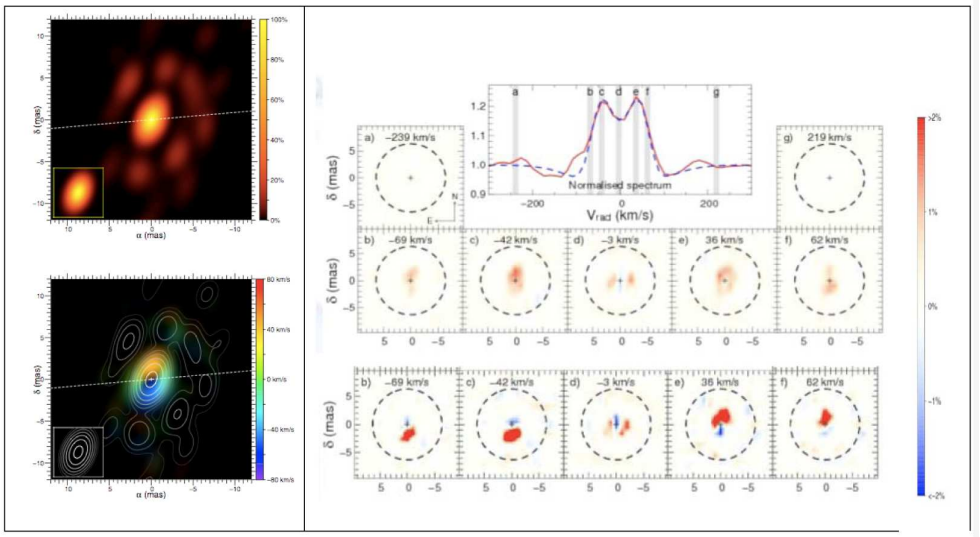

Figure 6: From Millour et al, A&A 2011: Polychromatic image reconstruction of the dust and wind around the A[e] star HD62623. Top left, classical image reconstruction in the continuum, revealing the skewed ring showing the inner part of the dust disc. Right, reconstruction of images in different spectral channels in the emission line, indicated by their relative "velocity". Top, classical image reconstruction, using the visibility and closure phase. The images reveal that the velocity bins have different angular sizes, but the closure phase gives a very weak constraint on the their position, which can lead to a completely wrong model. Bottom, polychromatic image reconstruction using the differential phases, as explained in figure 6. The dynamic of the images is very substantially improved and, more important, the location and shape of the velocity bins is much more accurate, leading to a very different model of quasi critical rotation with an axis very close to this expected from polarization measurements. The bottom left figure emphasizes the velocity field with a gray scale code corresponding to the radial velocity. The continuum image is only marginally modified by the polychromatic image reconstruction since the overall spectral coverage is very limited.

Figure 6 illustrates this procedure on the dust and wind around the A[e] star HD62623. The top left figure shows the "classical" image reconstruction in the continuum, from visibility and closure phases, revealing the skewed ring showing the inner part of the dust disc. The right figures show first the "classical" reconstruction of images in different spectral channels in the emission line. We see that the velocity bins have different angular sizes, but the closure phase gives a very weak constraint on the their position, which can lead to a completely wrong model. Bellow, we show a polychromatic image reconstruction using the differential phases, as explained in figure 5. The dynamic of the images is very substantially improved and, more important, the location and shape of the velocity bins is much more accurate, leading to a very different model of quasi critical rotation with an axis very close to this

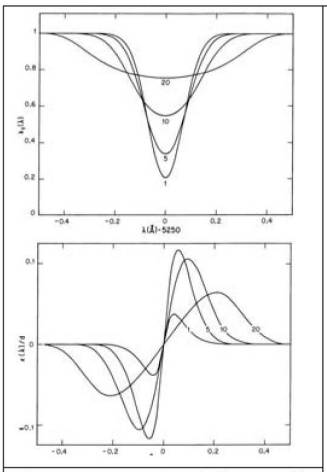

Figure 7a: Broadened line profile (top) and photocenter displacement, in stellar diameter units, (bottom) for stars rotating as solid bodies with velocities 1, 5, 10 and 20 km/s. The photocenter displacement is perpendicular to the rotation axis. From Chelli&Petrov, A&A1995.

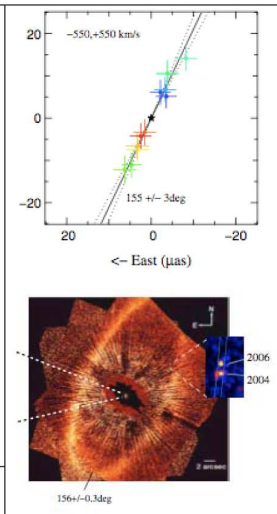

Figure 7b: (top) location of the photocenter displacement of Fomalhaut in different channels through the Brγ line (colors), relatively to the continuum photocenter (black) and (bottom), relationship with the debris disk of this star. From Le Bouquin et al, A&AL, 2009.

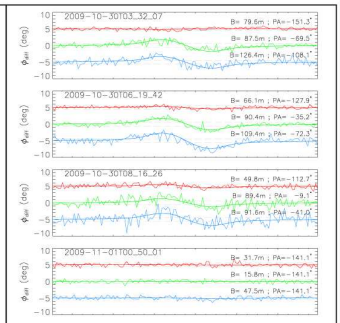

Figure 7c : High Spectral Resolution differential phase measures through the Brγ line on Achernar, for different baselines. A model fitting of these curves allowed to measure a diameter of 2.47 mas and a rotation velocity of 287 km/s on this unresolved object. Actually the differential phase is accurate enough to discuss the impact of Von Zeipel effect. From Domiciano et al, A&AL, 2012

Figure 7:

expected from polarization measurements. The bottom left figure emphasizes the velocity field with a color code corresponding to the radial velocity. The continuum image is only marginally modified by the polychromatic image reconstruction since the overall spectral coverage is very limited.

7. 1. NON RESOLVED SOURCES AND THE DIFFERENTIAL PHOTOCENTER

One remarkable feature of the differential phase is that it can be measured on very unresolved objects (Beckers 1982). If we make a development of the complex visibility function

$$O(\frac{\vec{B}}{\lambda},\lambda) - \int o(\vec{r},\lambda)e^{-2i\pi\frac{\vec{B}}{\lambda}\vec{r}}d\vec{r}$$

assuming that $\frac{\vec{B}}{\lambda}\vec{r}$ is always small when $o(\vec{r},\lambda)$ is non negligible (i.e. assuming that the object is unresolved), we get: $\phi(\lambda) = 2\pi\frac{\vec{B}}{\lambda}\vec{\varepsilon}(\lambda)$ where $\vec{\varepsilon}(\lambda) - \frac{\int \vec{r}o(\vec{r},\lambda)d\vec{r}}{\int o(\vec{r},\lambda)d\vec{r}}$ is the photocenter of the source brightness distribution (Petrov 1988). This quantity decreases only like the ratio $\frac{RB}{\lambda}$ between the source size ($R \propto \varepsilon(\lambda)$) and the interferometer resolution $\frac{\lambda}{B}$ and can be measured as soon as the SNR is sufficient. It is worth noting that 1-V(λ) decreases like $(\frac{RB}{\lambda})^2$ while the closure phase decreases like $(\frac{RB}{\lambda})^3$. So the

differential photocenter is the quantity that can be measured on the most unresolved objects. The use of the differential photocenter for unresolved objects has been proposed by Beckers (1982) for differential speckle interferometry and extended to long baseline interferometry (Petrov 1989). It has many applications: it can give the orientation (position angle) and constrain the size of any source for which spectral features are tentatively explained by a spatial distribution of elements at different velocities or with different spectra. In the case of rotating starts, it yields the orientation of the rotation axis (Beckers 1982), the angular diameter and the rotation velocity, independently from the Voigt line profile (Chelli & Petrov 1995). The rotation axis is of major importance in multiple systems, including star+planet pairs, where it can constrain the formation model and for stars with an accreting environment. These properties are illustrated by figures 7. In figure 7a, we see the predicted photocenter displacement in the direction perpendicular to the rotation axis, for different rotation velocities (Chelli & Petrov 1995). In figure 7b, we see the illustration of this effect on the measurement of the direction of the rotation axis of Fomalhaut, with a comparison with the known debris disk of this star (Le Bouquin et al. 2009). Figure 7c illustrates the measures that allowed the differential interferometry study of the diameter and rotation velocity of the unresolved star Achernar (Domiciano de Souza et al. 2012).

7. 2. THE SPECTRUM AND THE DIFFERENTIAL MEASURES

We have seen that the spectrum is necessary to calibrate the other interferometric observables. For non resolved sources, the spectrum is the zero order moment of the source brightness distribution while the photocenter displacement yields its first order moment. It has been shown (Chelli & Petrov 1995) that in rotating stars, combining the spectrum and the photocenter displacement allows to obtain quantities which depend only from the global geometry of the velocity field and are insensitive to the local "Voigt" line profile. More generally combining the study of the temporal evolution (or frequencies) of $\mathrm{s}(\lambda, \mathrm{t})$ with this of $\varepsilon(\lambda, \mathrm{t})$ allows interferometry to generalize, complement and validate Doppler Imaging. This has been demonstrated by numerical simulations in the case of star spots (Petrov 1988), non-radial stellar pulsations (Jankov et al. 2001) and inhomogeneous stellar surface abundances (Jankov et al. 2003). An efficient combination between the spectro-interferometric observables and the spectrum imply that the latest is measured simultaneously, with the same instrument and properly calibrated. This is why we consider the spectrum as one of the spectro-interferometric observables.

8. CONCLUSION

We have given examples of the spectro-interferometric use of all AMBER observables. We have shown that taking the spectral information into account at the very beginning of the information extraction process is not an additional problems but a real help both in terms of calibration accuracy and of information quantity. Many interferometric results have been obtained with single band interferometers, but we believe that, as most instruments are now spectro-interferometric, the spectral information will be systematically used. We also believe that the spectro-interferometric approach can make interferometry easier to approach for new users. Interferometric image reconstruction is a complex process and images will long remain rare and slow to obtain. On the other hand, astrophysicists are used to interpret spectra. Considering

that the spectro-interferometric variables are just integrals other the object brightness distribution, just has the spectrum, but with a different weighting of the different spatial components of the object might be much easier than having to apprehend all the subtleties of the aperture synthesis and image reconstruction.

9. ANNEX: AMBER AND THE VLTI

9. 1. THE VLTI

The VLTI (http://www.eso.org/sci/facilities/paranal/telescopes/vlti/, Glindemann et al. 2000, Glindemann et al. 2004) is the interferometric mode of the Very Large Telescope installed by ESO on Mount Paranal in Chile. It can combine up to 4 of the VLT apertures: the four 8 m telescopes called the UTs or the four 1.8 m auxiliary telescopes called the ATs. The UTs are fixed and the maximum baseline is 134 m between UT1 and UT4. The ATs are relocatable on a large number of stations, with a potential maximum baseline of 200 m, but currently the longest operational baseline is 139 m. The VLTI provides the beam collection, the partial correction of the local wave front errors, thanks to adaptive optics (MACAO on UTs) or to fast tip-tilt correctors (on the ATs), the beam transport, the OPD global equalization thanks to delay lines, the pupil and image stabilization in the focal laboratory. It is also stabilizes the OPDs within a fraction of λ (cophasing) or a fraction of the coherence length (coherencing) either on the observation source itself, if it is bright enough, or on an off axis source, if such a source exists. It is also supposed to measure very accurately the differential OPD between the on axis and the off axis source. When this PRIMA mode is operational, it will provide phase referencing (and hence absolute phases) and astrometry between the two sources.

The focal instruments are installed in the focal laboratory, where all beams are delivered and coherenced or cophased, if possible.

– VINCI: was a two telescope test instrument working in broad band in K. It allowed to test the VLTI and provided its first fringes in 2003, but also produced 47 science papers based on absolute visibility measurements. This still represents 22% of the science papers in spite of the fact that it has been decommissioned in 2005.

– MIDI: is the first general user VLTI focal instrument, and its first spectro-interferometer. It combines two telescopes in the N band (8 to 12 μm) and disperses the fringes with resolutions from 30 to 300. Until december 2012, It has produced close to 36% of the VLTI refereed science papers and will be maintained in operation until the installation of MATISSE in 2015.

– AMBER: is the second "first generation" general user VLTI instrument and is described in more details in the next section.

– PIONEER: is a "visitor" instrument currently used to demonstrate the 4 telescopes operation and potential of the VLTI and highlight its imaging capability. It works in the H band with a modest spectral dispersion of 35.

– GRAVITY: a "2$^{\rm nd}$ generation VLTI instrument" is a 4T beam combiner for the K band, with spectral resolutions 30, 450 and 1500. Its main goal is to allow extremely accurate astrometry in a small field around the galactic center, to detect relativistic signatures of the central Super Massive Black Hole. It will also be a high performance 4T spectro interferometer in the K band, around 2014.

– MATISSE: the other "2nd generation VLTI instrument" is a 4T beam combiner with an extremely large spectral coverage, from 3 to 13 μm (L,M and N) with resolutions ranging from 30 to 4500. It will be the most complex spectro interferometer on the VLTI.

– Some discussions about a 3rd generation of VLTI instruments are starting. One option is to extend the spectral coverage towards the visible, which will offer new science topics and increase the angular resolution.

9. 2. AMBER

AMBER (Petrov et al. 2007) is a "first generation" general user VLTI instrument. It works in the near infrared, in the K, H and J bands. It combines three telescopes (3UTs or 3ATs) and has three spectral resolution modes: R=35 (LR); R=1500 (MR) and R=12000 (HR). It has been explicitly designed to be a spectro-interferometer, with all the spectro-interferometric observables described in this paper and to have an imaging capability thanks to the possibility to measure closure phases. It has been designed in the late 1990s, is operational since 2004. It has produced 38% of all VLTI science published before december 2012, including the first images and many spectro-interferometric measures, with some examples in this paper. These design characteristics of AMBER, coupled to the VLTI potential, open up the access to investigations of initial science goals from solar system objects to extragalactic astronomy, including for instance: Asteroids, Stellar Fundamental Parameters, Stellar wind and Circum-stellar environments, Red Giants and Supergiants, Asymptotic Giants Branch stars (Cepheids and Distance scales, Miras), Planetary Nebulae, Wolf-Rayet stars, Luminous Blue Variables, Novae, Young Stellar Objects (Herbig Ae/Be stars, T Tauri stars, Massive Young Stellar Objects), Exoplanets, Galactic Center and Active Galactic Nuclei. All this scientific goals have already been achieved except, for the moment, Asteroids and Exoplanets.

The standard data processing of AMBER (Tatulli et al. 2007) assumes that the fringes are detected in each interferogram with a SNR>2. This assumes that the limiting magnitude for all higher spectral resolution modes is set by this of the fringe tracker needed to make exposures long enough to get above the detector read-out noise. It eventually appeared that the fringe tracker limiting magnitude (K=7.5 with the UTs) is much lower than the coherencing magnitude of AMBER, even with a resolution 1500. We have developed a new observation method and a new data processing, based on the accumulation of 2D Fourier power or cross spectra which allow to integrate a few seconds, or even minutes to detect and process the fringes. This allowed to reach K>10 in MR and K>11.5 in LR with the UTs (Petrov et al. 2012).

Acknowledgements

AMBER has been specified, designed and built for the VLTI by a consortium of european institutes: in France: University of Nice Sophia- Antipolis, University of Grenoble, Observatoire de la Côte d'Azur, INSU; in Germany: Max Planck Institute for Radioastronomie in Bonn; in Italy: Astrophysical Observatory of Arcetri in Firenze. (http://amber.obs.ujf-grenoble.fr/). The author is very gratefull to Slobodan Jankov for the extremely valuable editorial and scientific support to this paper.

References

Beckers, J. M.: 1982, *Optica Acta*, **29**, 361.

Benisty, M., Renard, S., Natta, A., Berger, J. P., Massi, F., et al.: 2011, *Astron. Astrophys.*, **531**, 84.

Chelli, A., Petrov, R. G.: 1995, *Astron. Astrophys.*, **109**, 401.

Chiavassa, A., Lacour, S., Millour, F., Driebe, T., Wittkowski, M., et al.: 2010, *Astron. Astrophys.*, **511**, 51.

Colavita, M. M. & Wizinowich, P. L.: 2003, *Proc. SPIE*, **4838**, 79, Wesley A. Traub, Ed.

Colavita, M. M., Wizinowich, P. L., Akeson, R. L.: 2004, *Proc. SPIE*, **5491**, 454, Wesley A. Traub, Bellingham, W.A., Eds.

Domiciano de Souza, A., Kervella, P., Jankov, S., Vakili, F., Ohishi, N., et al.: 2005, *Astron. Astrophys.*, **442**, 567.

Domiciano de Souza, A., Hadjara, M., Vakili, F., Bendjoya, P., Millour, F., et al.: 2012, *Astron. Astrophys.*, **545**, 130.

Glindemann, A., Abuter, R., Carbognani, F., Delplancke, F., Derie, F., et al.: 2000, *Proc. SPIE*, **4006**, 2, Pierre J. Lena, Andreas Quirrenbach, Eds.

Glindemann, A., Albertsen, M., Andolfato, L., Avila, G., Ballester, P., et al.: 2004, *Proc. SPIE*, **5491**, 447, Wesley A. Traub, Ed.

Jankov, S., Vakili, F. Dominiciano de Souza, Jr., Janot-Pacheco, E.: 2001, *Astron. Astrophys.*, **377**, 721.

Jankov, S., Domiciano de Souza, A., Jr., Stehle, C., Vakili, F., Perraut-Rousselet, K., Chesneau, O.: 2003, *Proc. SPIE*, **4838**, 587, Wesley A. Traub, Ed.

Le Bouquin, J.-B., Absil, O., Benisty, M., Massi, F., Mérand, A., Stefl, S.: 2009, *Astron. Astrophys.*, **498**, L41.

Malbet, F., Benisty, M., deWit, W.-J., Kraus, S., Meilland, A., et al.: 2007, *Astron. Astrophys.*, **464**, 43.

Meilland, A., Stee, P., Vannier, M., Millour, F., Domiciano de Souza, A., et al.: 2007, *Astron. Astrophys.*, **464**, 59.

Michelson, A. A., Pease, F. G.: 1921, *Astrophys. J.*, **53**, 249.

Millour, F., Meilland, A., Chesneau, O., Stee, Ph., Kanaan, S., et al.: 2011, *Astron. Astrophys.*, **526**, 107.

Monnier, J. D., Zhao, M., Pedretti, E., Thureau, N., Ireland, M., et al.: 2007, *Science*, **317**, 342.

Petrov, R. G: 1988, *ESOC*, **29**, 235.

Petrov, R. G.: 1989, *Diffraction-Limited Imaging with Very Large Telescopes, Proceedings of the NATO Advanced Study Institute, eds. D. M. Alloin, J. M. Mariotti (Kluwer)*, **274**, p. 249.

Petrov, R. G., Malbet, F., Weigelt, G., Antonelli, P., Beckmann, U., et al.: 2007, *Astron. Astrophys.*, **464**, 1.

Petrov, R. G., Millour, F., Lagarde, S., Vannier, M., Rakshit, S., et al.: 2012, *Proc. SPIE*, **8445**, 0WP.

Stee, Ph.: 1996, *Astron. Astrophys.*, **311**, 945.

Tatulli, E., Millour, F., Chelli, A., Duvert, G., Acke, B., et al.: 2007, *Astron. Astrophys.*, **464**, 29.

Weigelt, G., Grinin, V. P., Groh, J. H., Hofmann, K.-H., Kraus, S., at al.: 2011, *Astron. Astrophys.*, **527**, 103.

Woillez, J., Akeson, R., Colavita, M., Eisner, J., Millan-Gabet, R. et al.: 2012, *Publ. Astron. Soc. Pac.*, **124**, 51.